

Electronic Supplementary Information (ESI)

Electrodeposition of indium from the ionic liquid trihexyl(tetradecyl)phosphonium chloride

Clio Deferm, João C. Malaquias, Bieke Onghena, Dipanjan Banerjee, Jan Luyten, Harald Oosterhof,
Jan Fransaer and Koen Binnemans*

Experimental

Chemicals

Trihexyl(tetradecyl)phosphonium chloride (Cyphos® IL 101, purity >97%), Trihexylphosphine (Cytop® 360) and Cyanex® 923 (a mixture of four trialkylphosphine oxides) were purchased from Cytec Industries Inc. (Niagara Falls, Ontario, Canada). $\text{InCl}_3 \cdot 4\text{H}_2\text{O}$ (99.99%) was obtained from abcr (Karlsruhe, Germany). InCl_2 (99.9%), InCl (99.999%), ferrocene (98%), and CDCl_3 (99.8 atom% D) were obtained from Fluka (Sigma-Aldrich, Diegem, Belgium). The 0.1 M NaOH solution (AVS TITRINORM®), HCl (Analar Normapur, 37%) and ZnCl_2 (98%) were purchased from VWR (Leuven, Belgium). NH_3 (a.r., 25%), heptane (99+% C_7H_{16} , mixture of isomers), acetone (99+%), phosphoric acid (85% p.a.) and lanthanum and gallium standard (1000 ppm in 3–5 wt% nitric acid) were purchased from Chem-Lab (Zedelgem, Belgium). FeCl_3 (98%) was purchased from Acros Organics (Thermo Fisher Scientific, Geel, Belgium). All chemicals, with the exception of Cyphos® IL 101, were used as received, without any further purification.

Instrumentation and analysis methods

All the electrochemical experiments were carried out using a three-electrode setup in an argon-filled glovebox (Glovebox Technologies Limited). Oxygen and water contents were kept below 1 ppm at all times. For cyclic voltammetry experiments the counter electrode used was a molybdenum plate. The working electrodes used were platinum-coated silicon wafers (silicon covered with 500 nm of silica, 10 nm of titanium and 100 nm of platinum, $0.32 \pm 0.10 \text{ cm}^2$) and molybdenum-coated soda lime glass substrates (500 nm, $0.31 \pm 0.08 \text{ cm}^2$). The cathodic (E_{red}) and anodic (E_{ox}) limiting potentials were determined by a graphical method at the potential value where tangent lines to the main reduction/oxidation peaks and the horizontal baseline at the “flat” electroactivity domains cross. Redox reaction potentials were determined by the same method. The limiting potentials of the electrochemical window are represented in the figures by vertical dashed lines. Unless stated otherwise, all cyclic voltammograms (CVs) were measured starting at open circuit potential (OCP) and scanning first in the cathodic direction.

The rotating ring disk electrode experiments were conducted using a platinum disk ($\varnothing = 4.57 \text{ mm}$) and ring ($\varnothing_{\text{inner}} = 4.93 \text{ mm}$, $\varnothing_{\text{outer}} = 5.38 \text{ mm}$, both 99.99% Pt, mirror polished, Pine Instrument E7R8 RRDE tips), separated by an insulating PTFE thin gap (180 μm). A collection efficiency of 20.4% was used, determined by Vanhoutte *et al.*¹ The electrode tip was $\pm 0.5 \text{ cm}$ deep in the electrolyte. A molybdenum plate was used as counter electrode. For the determination of the diffusion coefficient, a platinum rotating disk electrode (Metrohm Autolab RDE, $\varnothing = 5 \text{ mm}$) embedded in PEEK was used.

For the deposition of indium thin films, a molybdenum plate was used as counter electrode and molybdenum-coated soda lime glass substrates ($0.50 \pm 0.05 \text{ cm}^2$) as working electrodes. The morphology and elemental composition of the films were analyzed by scanning electron microscopy (SEM; Phillips XL-30 FEG) and energy-dispersive X-ray spectroscopy (EDS; Octane elite super silicon drift detector, Ametek EDAX). For supercritical drying, the deposits were, immediately after being taken out of the glovebox, submerged in acetone (to remove traces of ionic liquid) for 2 days before the acetone was gradually replaced by isopropanol. Super critical drying was executed by a Tousimis Autosamdri®-815B critical point dryer. The sample was flushed for 10 min with CO_2 before the critical point was reached.

For the formation of indium microparticles in solution, a platinum plate was used as the working electrode (0.80 cm^2). Afterwards, 1 mL of ionic liquid containing the indium microparticles was dissolved in 20 mL of acetone. As soon as the indium particles were settled on the bottom of the glass container, the acetone was removed as much as possible. The remaining liquid containing the indium particles was again diluted with acetone. These actions were repeated four times to decrease the ionic liquid concentration in the acetone even further

before three drops of the acetone solution were placed on a platinum working electrode and left to dry for SEM imaging.

The mass increase during deposition was measured using an electrochemical quartz crystal microbalance (Inficon, Maxtek RQCM). A custom-made electrochemical cell was used to perform measurements with small quantities of electrolyte (approx. 5 mL). This cell was placed inside an argon-filled glove box with oxygen and water concentrations below 1 ppm. A platinum substrate electrode on an Inficon AT-cut quartz crystal (1 inch, 90 °C) with a resonance frequency of 5 MHz and an electrochemical active surface area of 1.27 cm² was used as working electrode and a platinum wire as counter electrode. Frequency changes were converted to mass changes in accordance with Sauerbrey's equation.

For all electrochemical experiments, a platinum wire immersed in an equimolar solution of ferrocene-ferrocenium in the ionic liquid [BMP][Tf₂N] was used as reference electrode. The concentration of the ferrocene-ferrocenium redox couple was 10 mM and the [BMP][Tf₂N] containing the redox couple was placed inside a glass tube with a glass frit on the bottom.^{2,3} 10 mM ferrocene was dissolved in [BMP][Tf₂N] and subsequently 5 mM ferrocene was electrochemically oxidized to ferrocenium. Before the experiments, the platinum substrates were rinsed for 5 min with hydrochloric acid (6 N), deionized water and acetone and finally dried in a stream of hot air. The molybdenum substrates were etched for 5 min with ammonia solution (6 N), rinsed with deionized water and acetone and finally dried in a stream of hot air. The electrochemical experiments were performed using a Metrohm Autolab PGSTAT 302N potentiostat controlled by NOVA 1.11 software.

The composition of the indium–zinc–iron deposits was determined using a bench top total reflection X-ray fluorescence spectrometer (TXRF; Bruker S2 Picofox). Each of the deposits, deposited on a molybdenum working electrode, were dissolved in 500 µL of a 6M HCl solution prior to analysis. Afterwards, an aliquot of the HCl solution was mixed with lanthanum and gallium internal standard solutions, and ultrapure water until a total volume of 1 mL was obtained. In order to create a hydrophobic surface, the quartz glass sample carriers were first treated with 30 µL of a silicone solution in isopropanol and dried for 30 min in a hot air oven at 60 °C. Afterwards, 5 µL of the sample was added and the carriers were dried for 1 h at 60 °C. The metal concentrations in the aqueous phase were measured for 1000 s.

³¹P NMR spectra were recorded on a Bruker Avance™ II 600 MHz NMR spectrometer, operating at 243 MHz. Samples were dissolved in CDCl₃. ³¹P NMR spectra were measured with respect to a H₃PO₄ external reference (25 vol% in water). A delay time (d1) of 5 s was applied in the NMR pulse sequence and 325 scans were recorded. The NMR spectra were analyzed using TopSpin 3.5 software.

The viscosity of the organic phase was measured using a rolling-ball type viscometer (Anton Paar, Lovis 2000 ME), densities were determined using a density meter with an oscillating U-tube sensor (Anton Paar, DMA 4500 M)

Differential scanning calorimetry (DSC) scans were recorded on a TA Instruments DSC-2920 (cooled with liquid nitrogen) in sealed aluminum crucibles with a heating rate of 5 °C min⁻¹ and a nitrogen gas flow of 60 mL min⁻¹.

For determining dewetting behavior, a uniform indium thin film was deposited on molybdenum from an InCl₃ aqueous bath by using a current density of 250 mA cm⁻² and a low deposition-bath temperature of -5 °C, according to the procedure described by Lobaccaro *et al.*⁴ The indium deposit was fused into glass under vacuum and heated in a vacuum oven (Binder VD series) at 100 °C for 24 h. The morphology and elemental composition of the deposit was analyzed by SEM imaging before and after heating.

Extended X-ray Absorption Fine Structure (EXAFS) spectra of the indium K-edge (27 941 eV) were collected at the Dutch-Belgian Beamline (DUBBLE, BM26A) at the European Synchrotron Radiation Facility (ESRF) in Grenoble (France).⁵ The energy of the X-ray beam was tuned by a double-crystal monochromator operating in fixed-exit mode using a Si(111) crystal pair. The measurements were done in transmission mode using Ar/He gas-filled ionization chambers at ambient pressure. Plastic cuvettes with a path length of 2 or 5 mm were used. One scan was recorded per sample. Viper software was used for isolating the EXAFS function (χ), using standard procedures for pre-edge subtraction and data normalization and subtraction of the atomic background with a smoothing spline.⁶ The EXAFS functions were all k^3 – weighed and Fourier transformed over the k -range from 3 to 16 Å⁻¹. The data were fitted with a model consisting of one In–Cl bond. The *ab initio* code FEFF 7.0 was used to calculate the theoretical phase and amplitude functions that were subsequently used in the non-linear least-squares refinement of the experimental data.⁷ The EXAFS data were fitted in $R + \Delta$ (Å) space between 0 and 2.42 Å without window function. Estimated standard deviations are shown in parentheses and calculated by VIPER. The amplitude reduction factor S_0 was fixed to 0.9, which was deduced by fitting the main species present in the three reference samples of indium(III) chloride in 1-methyl-3-octylimidazolium chloride. Both the references and the samples were prepared by dissolving indium(III) chloride in either 1-methyl-3-octylimidazolium chloride, for the references, or Cyphos IL 101, for the samples, in three different ratios, followed by drying for three days on a Schlenk line at 60 °C and are labeled according to the mole fraction of indium(III) chloride in the mixture: $x\text{InCl}_3 = 0.20, 0.25$ and 0.33 . The main species in these references were $[\text{InCl}_6]^{3-}$, $[\text{InCl}_6]^{3-}$ and $[\text{InCl}_5]^{2-}$, respectively.

Purification of Cyphos IL 101

The commercial ionic liquid Cyphos IL 101 (purity: >97%) was purified according to a literature method: washing with a 0.1 M NaOH solution, washing with water until the pH was neutral, followed by multiple reflux steps using hot heptane.⁸ The amount of impurities was estimated by comparing the integration of the impurities ³¹P resonance signal, to the integration of the ³¹P resonance signal of the trihexyl(tetradecyl)phosphonium cation at 33.5 ppm. The ionic liquid was thoroughly dried for 4 h under vacuum (<1 mbar) on a rotary evaporator (80 °C) and on a Schlenk line at 60 °C for several days. Purity: > 99.5% Yield: 72%.

The thermal stability of Cyphos IL 101 under different conditions (temperature, atmosphere and metal loading) was examined in previous work.⁵¹ The ionic liquid is thermally stable under the conditions chosen for the electrochemical experiments.

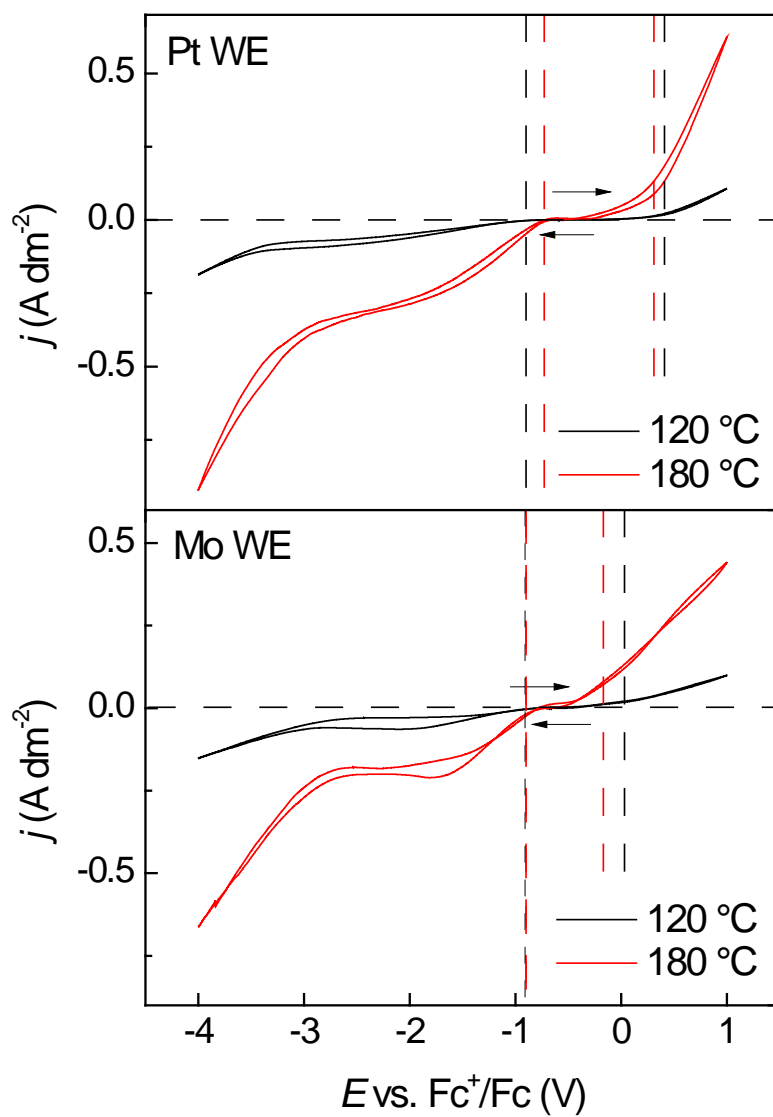


Fig. S1 CVs (1st cycle) of commercial Cyphos IL 101 recorded on a platinum working electrode (WE) and a molybdenum working electrode (WE) at 120 °C and 180 °C. Scans were recorded at $v_{\text{scan}} = 20 \text{ mV s}^{-1}$.

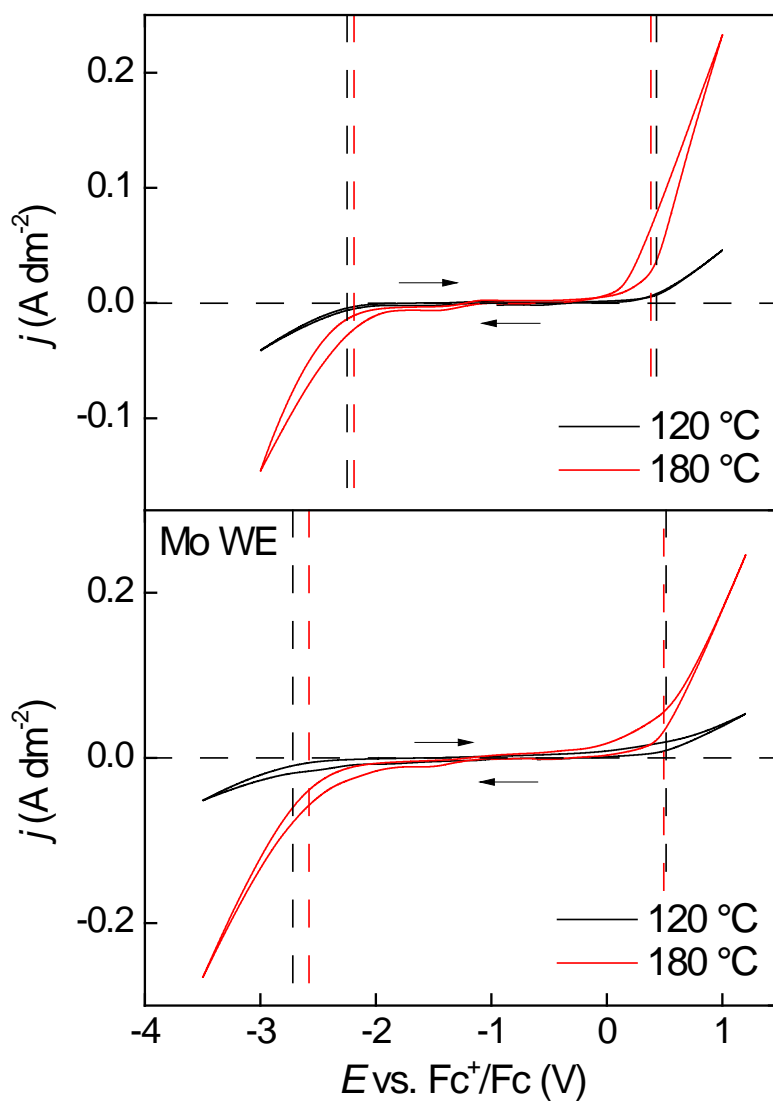


Fig. S2 CVs (1st cycle) of purified Cyphos IL 101 recorded on a platinum electrode (WE) and a molybdenum working electrode (WE) at 120 °C and 180 °C. Scans were recorded at $v_{\text{scan}} = 20 \text{ mV s}^{-1}$.

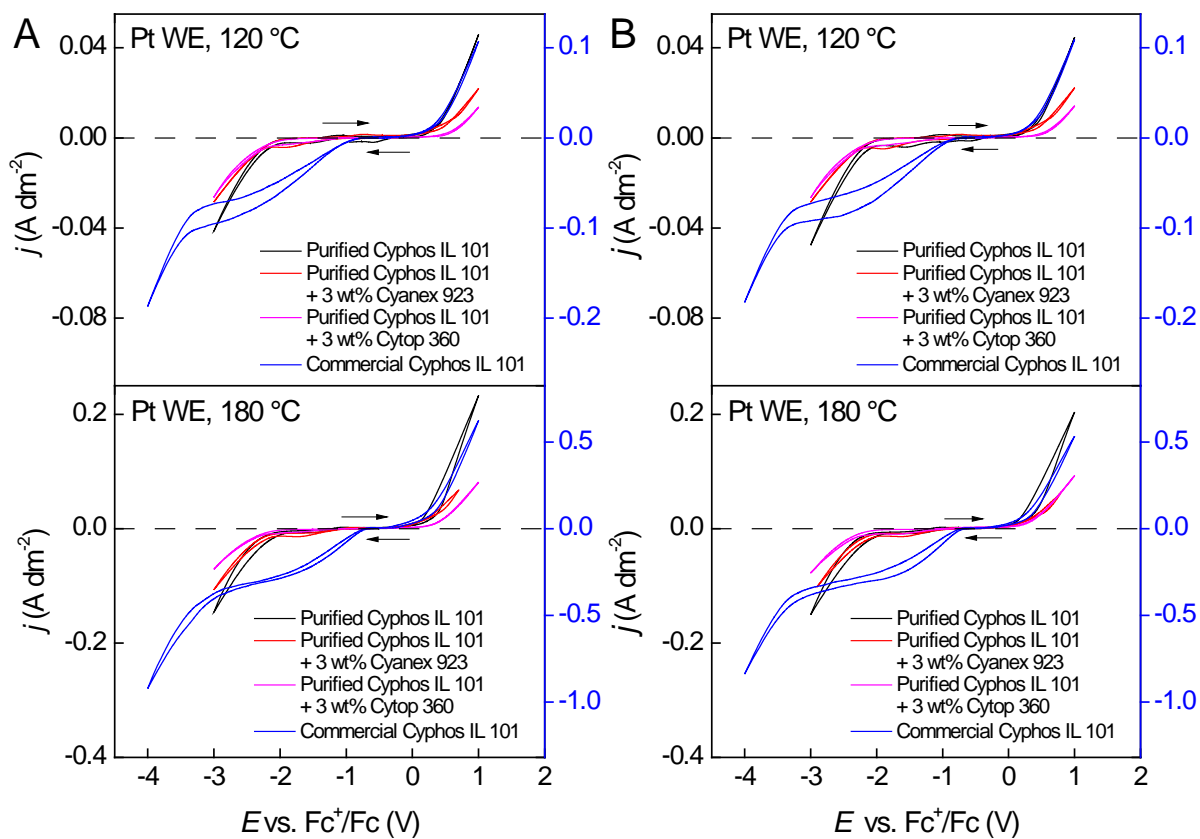


Fig. S3 CVs (A: 1st cycle, B: 2nd cycle) of purified Cyphos IL 101, purified Cyphos IL 101 containing 3 wt% of Cyanex 923 or Cytop 360 and commercial Cyphos IL 101 (blue axis) recorded on a platinum working electrode (WE) at 120 °C and 180 °C. Scans were recorded at $v_{scan} = 20 \text{ mV s}^{-1}$.

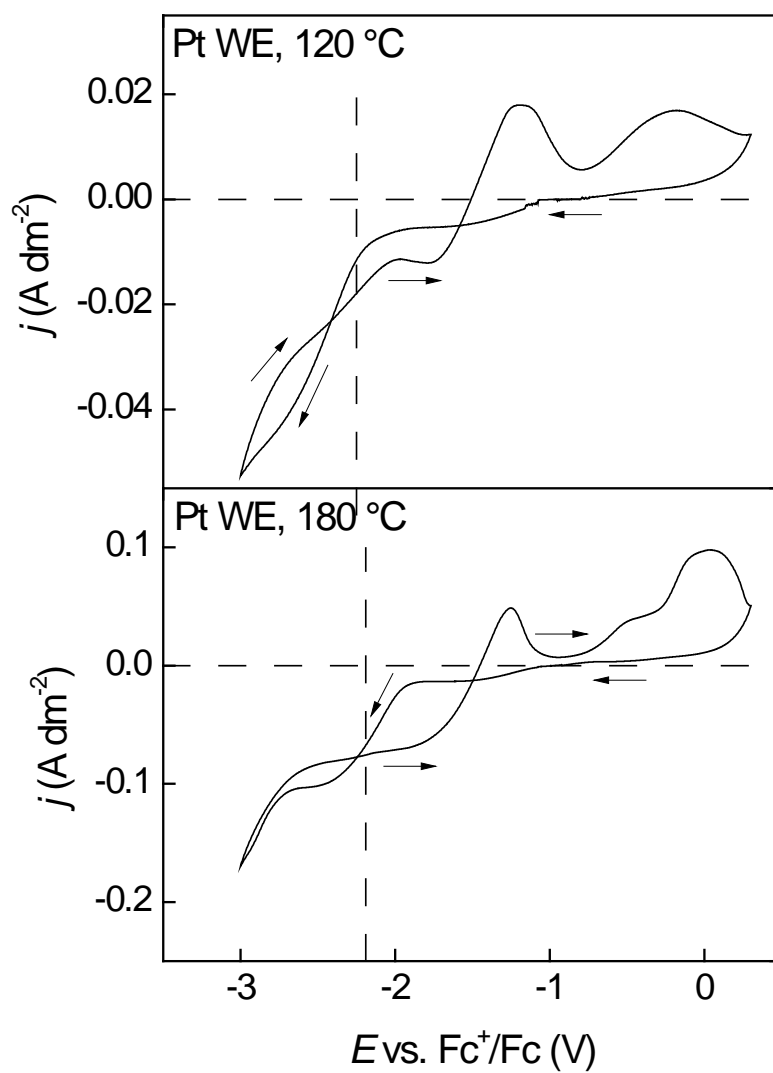


Fig. S4 CVs (1st cycle) of purified Cyphos IL 101 loaded with 10 mM of indium(III) on a platinum working electrode (WE) at 120 °C and 180 °C. Scans were recorded at $v_{scan} = 20\ mV\ s^{-1}$.

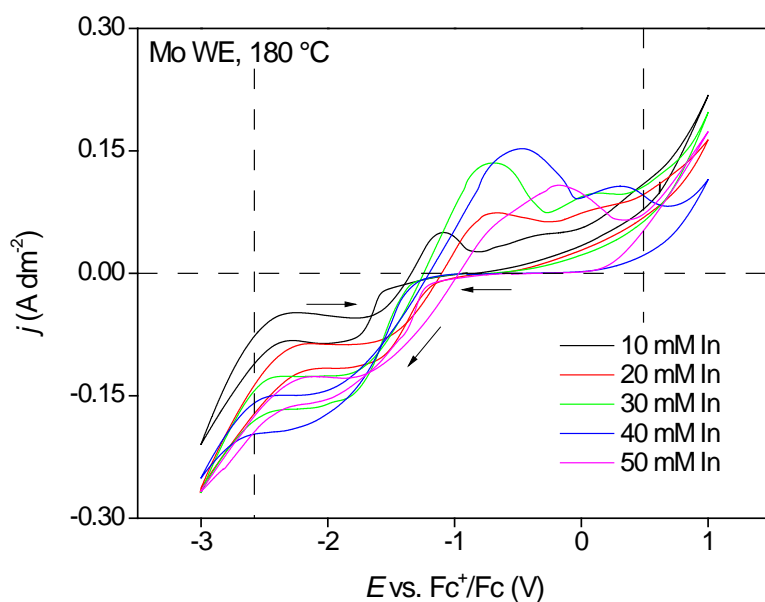


Fig. S5 CVs of purified Cyphos IL 101 loaded with 10, 20, 30, 40 and 50 mM of indium(III) on a molybdenum working electrode (WE) at 180 °C (1st cycle). Scans were recorded at $v_{\text{scan}} = 20 \text{ mV s}^{-1}$. A new working electrode was used for each measurement.

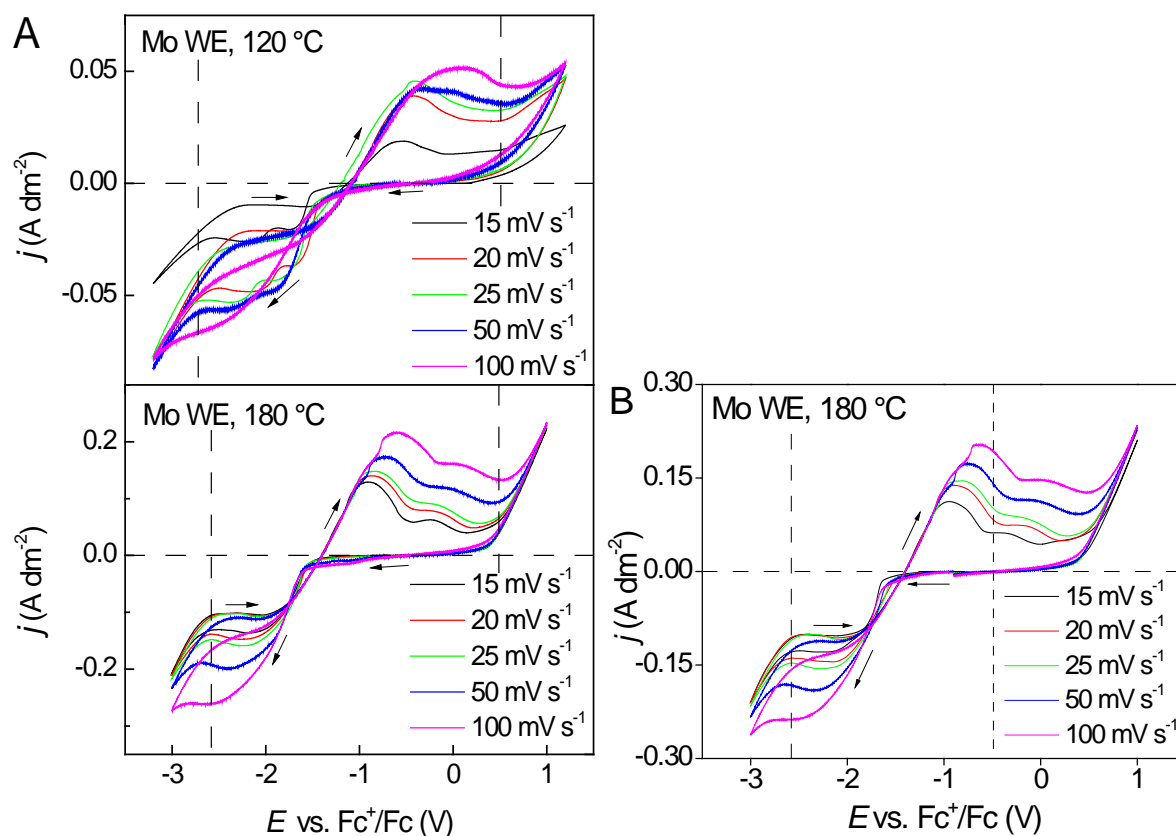


Fig. S6 CVs of purified Cyphos IL 101 loaded with 30 mM of indium(III) on a molybdenum working electrode (WE) (A: 120 °C (1st cycle) and 180 °C (2nd cycle), B: 180 °C (1st cycle). Scans were recorded at $v_{\text{scan}} = 20 \text{ mV s}^{-1}$.



Fig. S7 Purified Cyphos IL 101 containing 30 mM of indium(I) (A) and 30 mM of indium(II) (B). A small piece of solid grey material can be observed on the bottom of the flask.

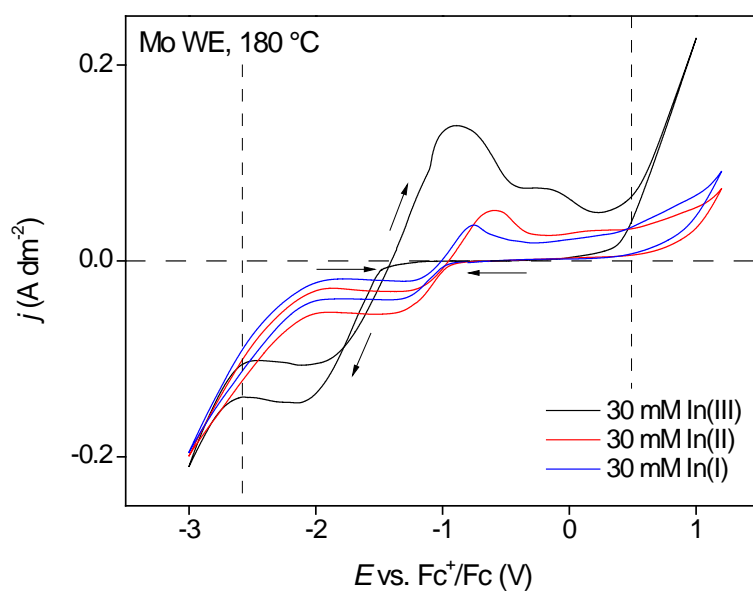


Fig. S8 CVs of purified Cyphos IL 101 loaded with 30 mM of indium(I), indium(II) or indium(III) on a molybdenum working electrode (WE) at 180 °C (1st cycle). Scans were recorded at $v_{\text{scan}} = 20 \text{ mV s}^{-1}$.

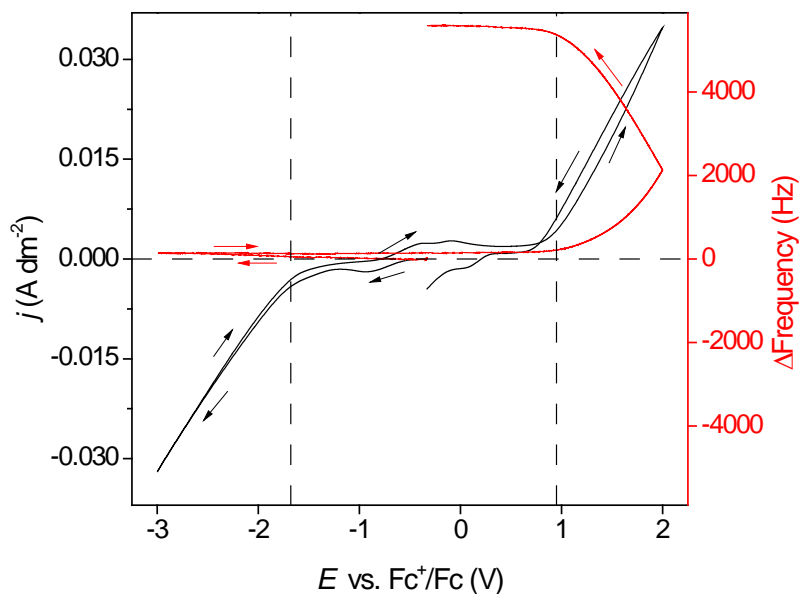


Fig. S9 CV (2nd cycle) of purified Cyphos IL 101 on a platinum working electrode at 120 °C (black line, left axis) with EQCM analysis (red line, right axis) Scans were recorded at $v_{\text{scan}} = 2 \text{ mV s}^{-1}$.

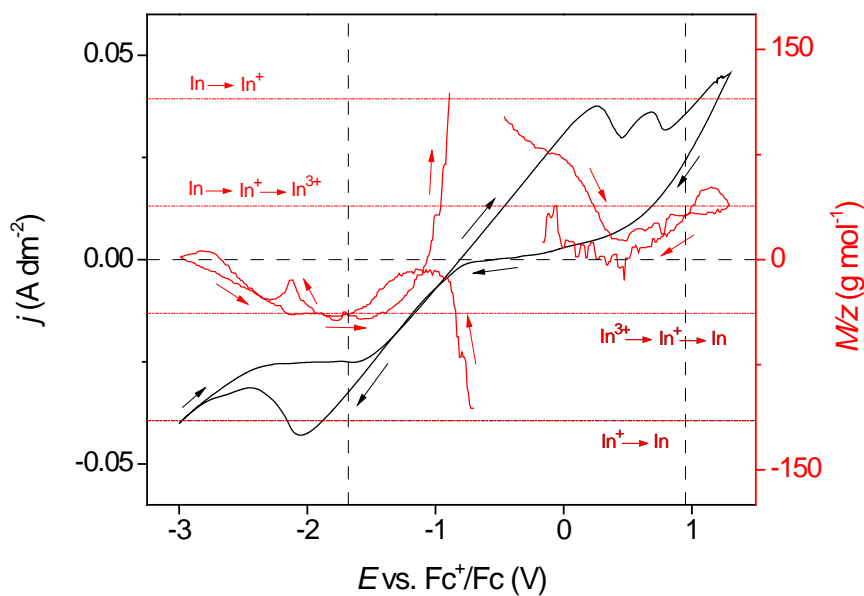


Fig. S10 CV (2nd cycle) of purified Cyphos IL 101 loaded with 50 mM of indium(III) on a Pt working electrode at 120 °C (black line, left axis) with EQCM data analyzed for M/z (red line, right axis) Scans were recorded at $v_{\text{scan}} = 2 \text{ mV s}^{-1}$. The EQCM data analyzed for M/z was smoothed by a 50% percentile filter with a 5 points window size.

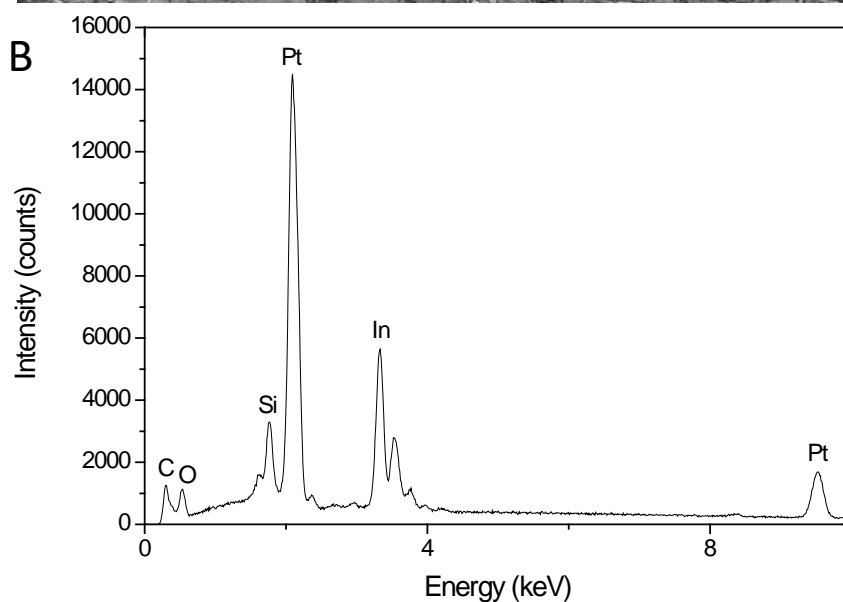
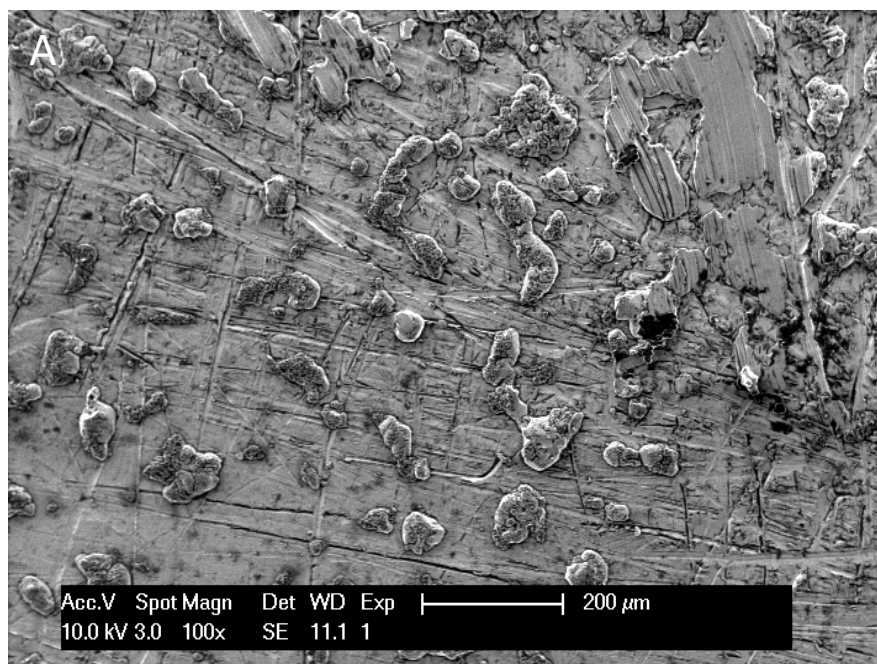


Fig. S11 SEM picture (A) and corresponding EDS spectrum (B) of indium deposited on a platinum working electrode at -1.65 V vs. Fc^+/Fc and at 120 °C for 18 h from purified Cyphos IL 101 loaded with 400 mM of indium(III).

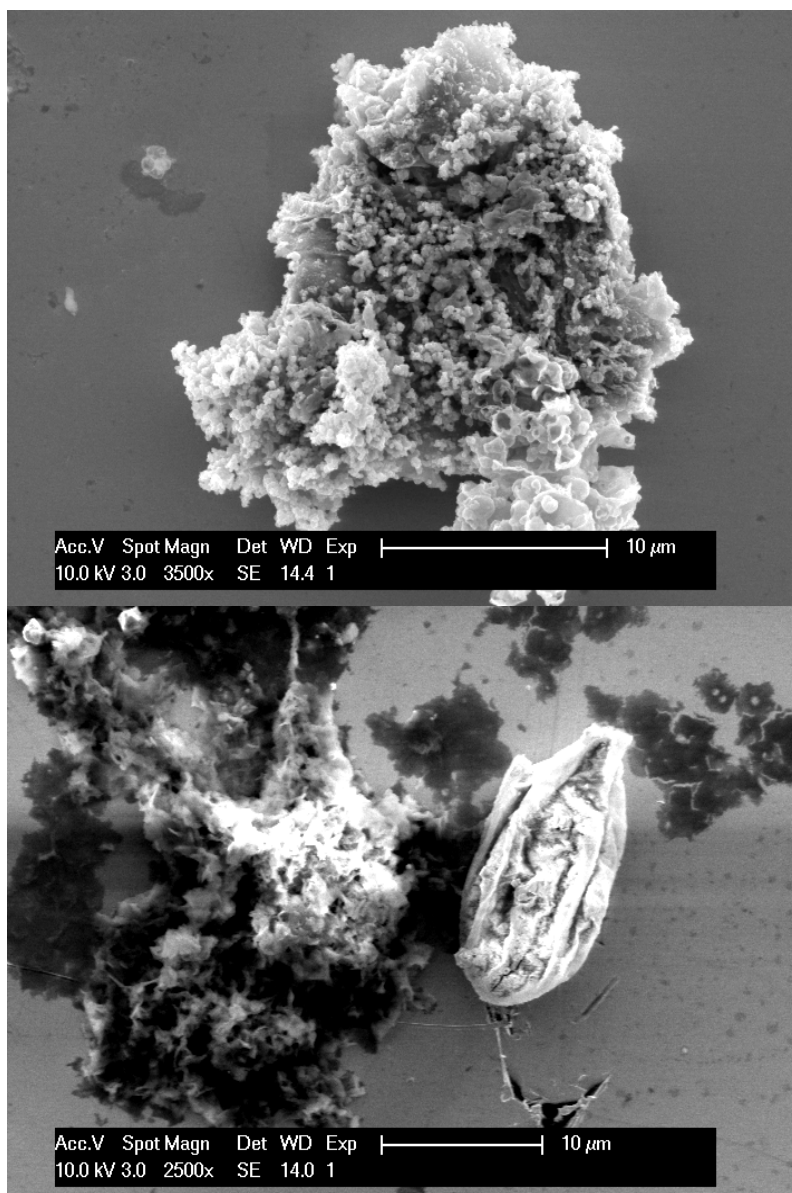


Fig. S12 SEM pictures of indium 'chunks' observed inside the electrolyte after a chronoamperometric experiment with a platinum working electrode at -1.65 V vs. Fc^+/Fc at 120 °C for 18 h from purified Cyphos IL 101 loaded with 400 mM of indium(III).

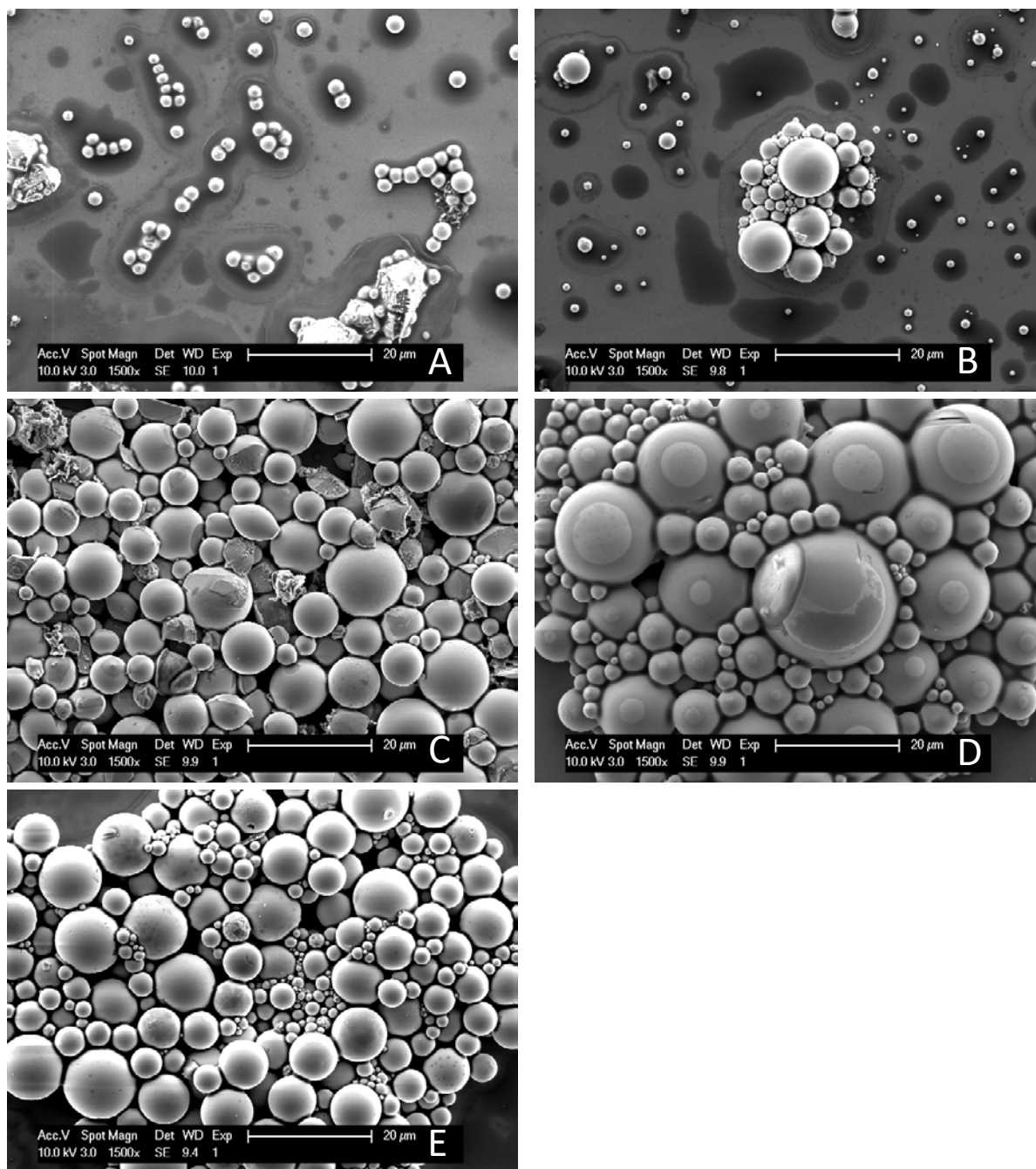


Fig. S13 SEM picture of indium deposited on a molybdenum working electrode at -2 V vs. Fc^+/Fc and for 2 h from purified Cyphos IL 101 loaded with 400 mM of indium(III) as a function of the temperature: 100 °C (A), 120 °C (B), 140 °C (C), 160 °C (D), 180 °C (E).

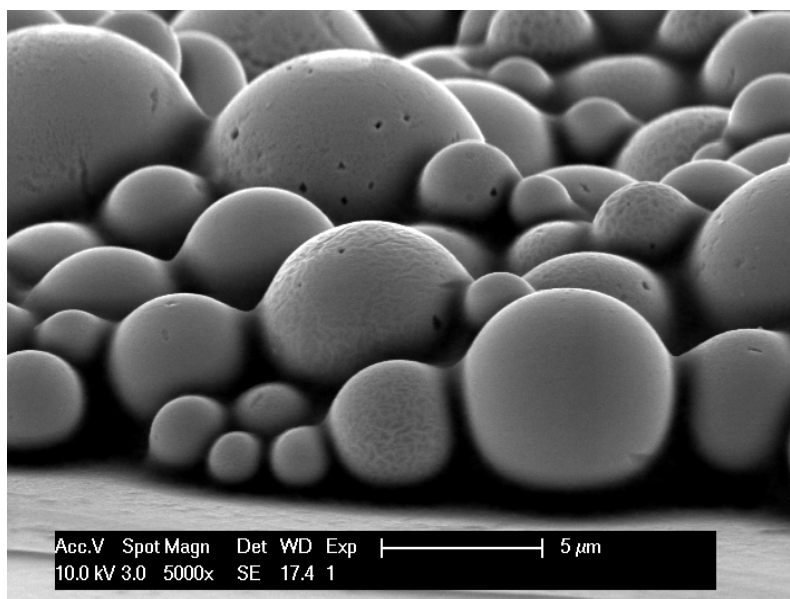


Fig. S14 SEM picture taken at an angle of 70° with the normal of indium deposited on a molybdenum working electrode at -2.00 V vs. Fc^+/Fc at 160°C for 2 h from purified Cyphos IL 101 loaded with 400 mM of indium(III).



Fig. S15 Indium deposits on a molybdenum working electrode from an InCl_3 aqueous bath by using a high current density of 250 mA cm^{-2} and a low deposition-bath temperature of -5°C unfused (A) and fused in glass under vacuum (B).

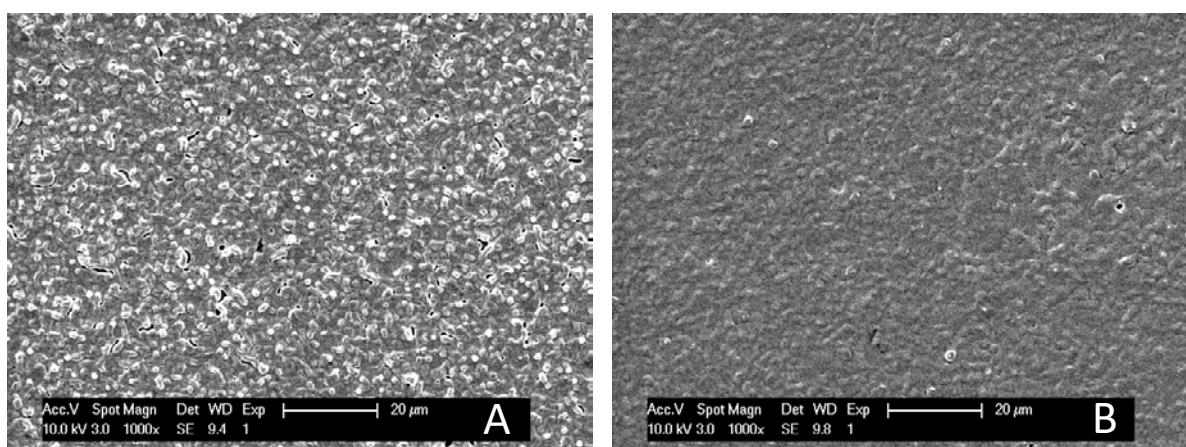


Fig. S16 Indium deposits on a molybdenum working electrode from an InCl_3 aqueous bath by using a high current density of 250 mA cm^{-2} and a low deposition-bath temperature of -5°C before (A) and after heating in a vacuum oven at 100°C for 24 h (B).

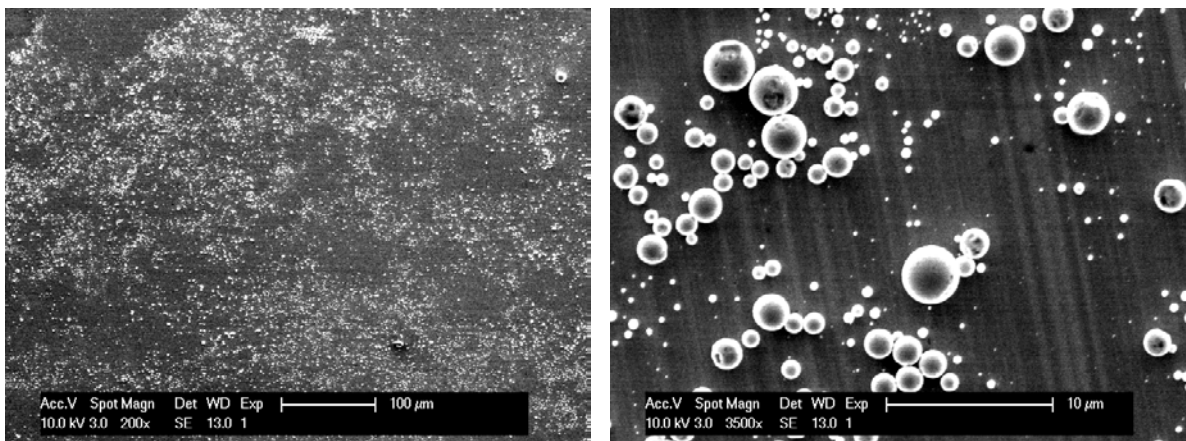


Fig. S17 SEM picture of indium deposited on a molybdenum working electrode at -2 V vs. Fc^+/Fc and for 2 h from purified Cyphos IL 101 loaded with 400 mM of indium(III) at 180 °C after supercritical drying.

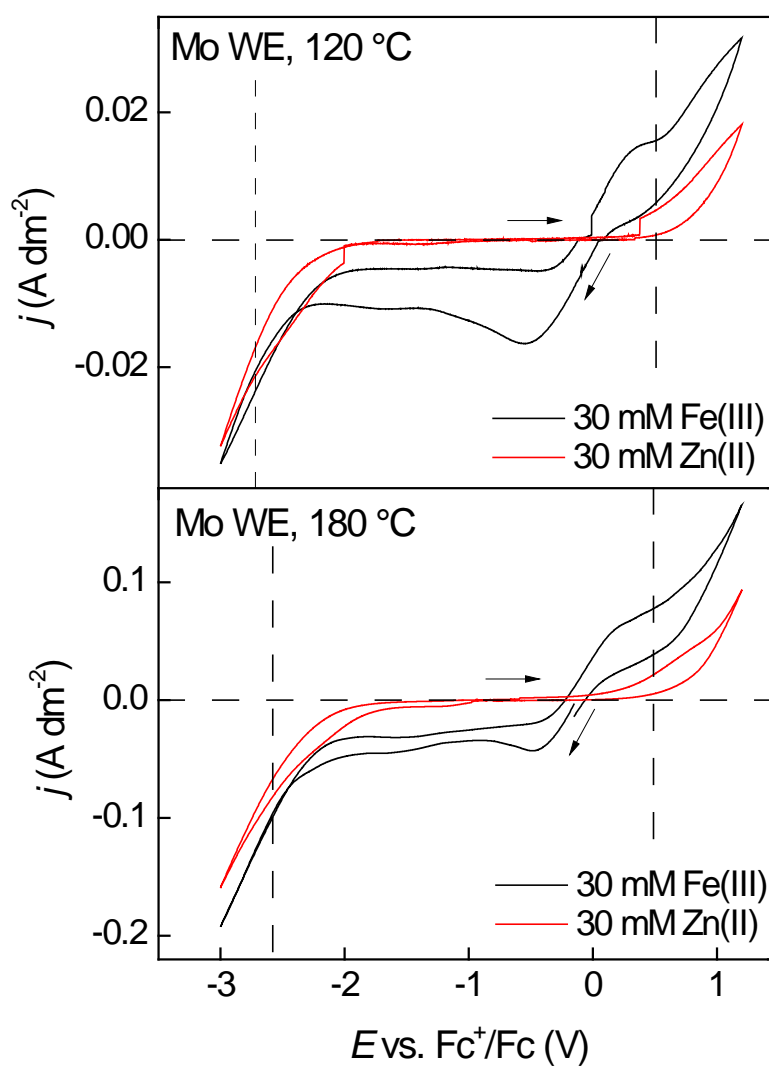


Fig. S18 CVs (2nd cycle) of purified Cyphos IL 101 loaded with 30 mM of zinc(II) or iron(III) on a molybdenum working electrode (WE) at 120 °C and 180 °C. Scans were recorded at $v_{\text{scan}} = 20 \text{ mV s}^{-1}$.

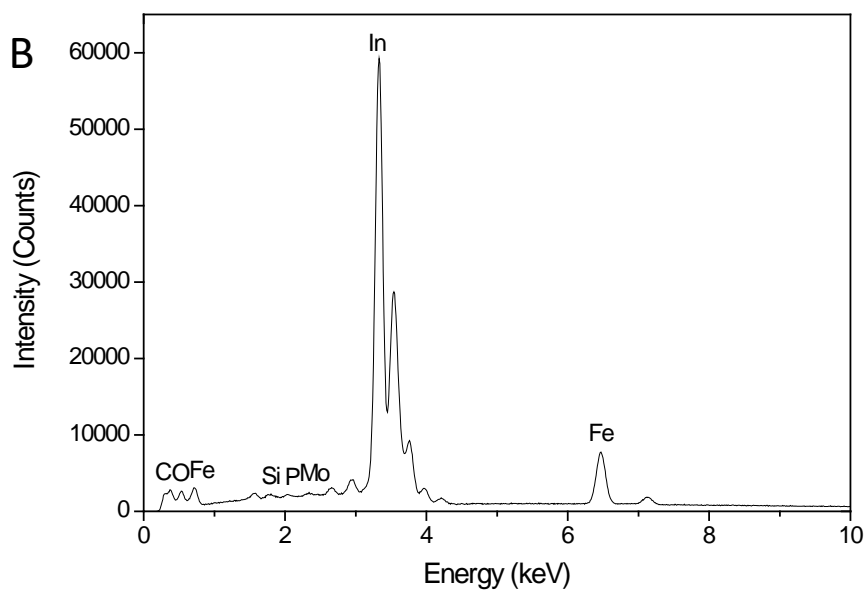
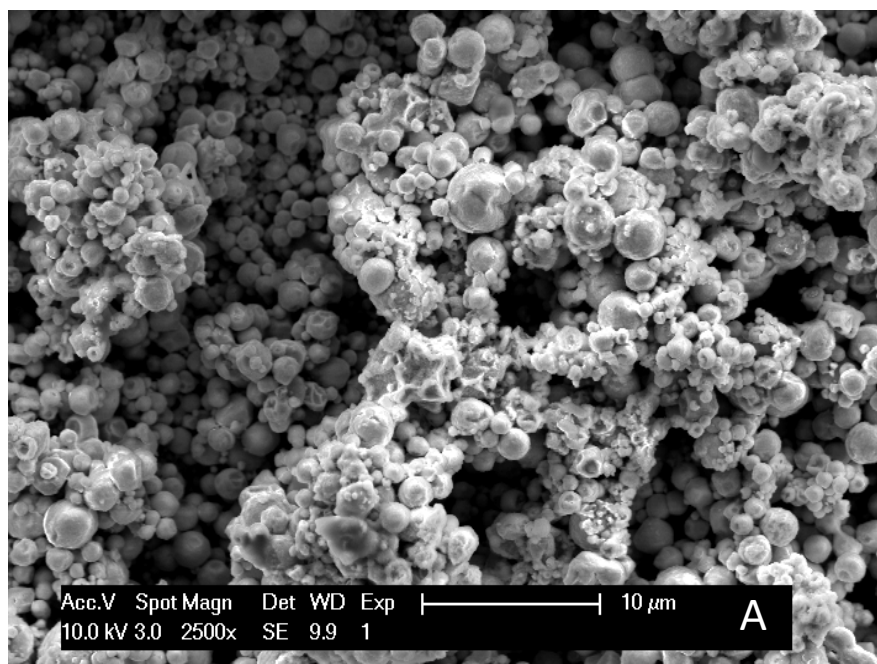


Fig. S19 SEM picture (A) and corresponding EDS spectrum (B) of deposits on a molybdenum working electrode at -1.80 V vs. Fc^+/Fc and at 120 °C for 3 h from purified Cyphos IL 101 loaded with 400 mM of indium(III), 400 mM of zinc(II) and 400 mM of iron(III).

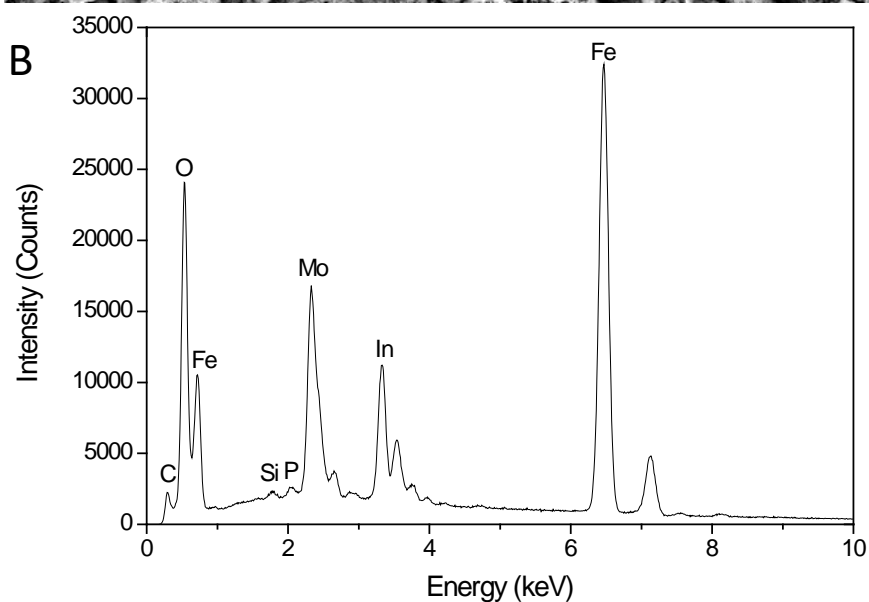
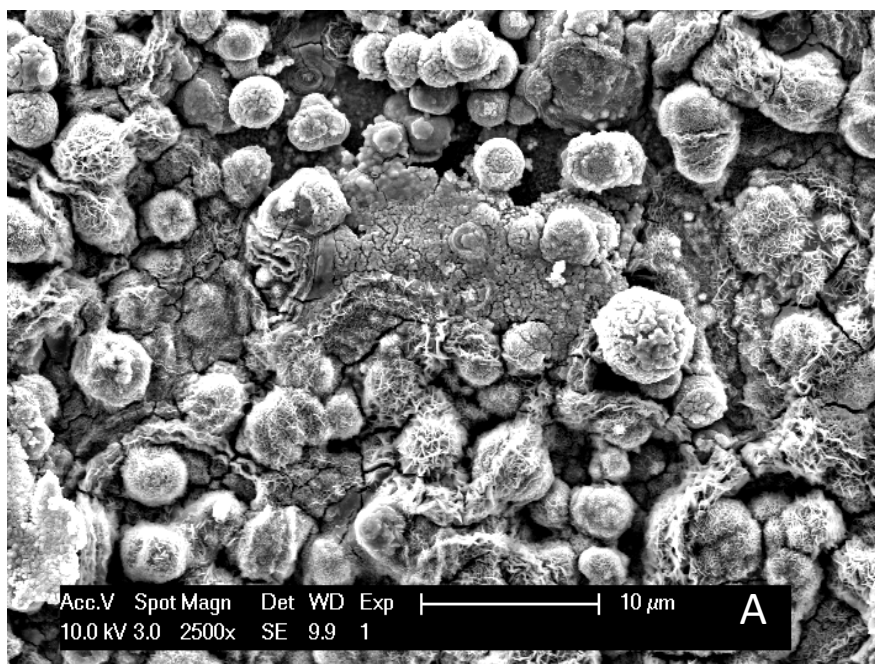


Fig. S20 SEM picture (A) and corresponding EDS spectrum (B) of deposits on a molybdenum working electrode at -1.80 V vs. Fc^+/Fc and at 180 °C for 3 h from purified Cyphos IL 101 loaded with 400 mM of indium(III), 400 mM of zinc(II) and 400 mM of iron(III).

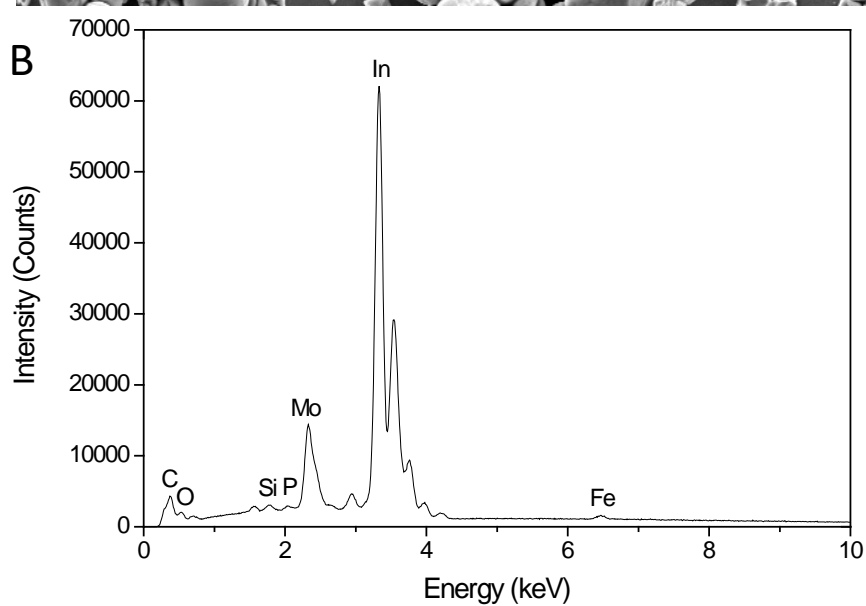
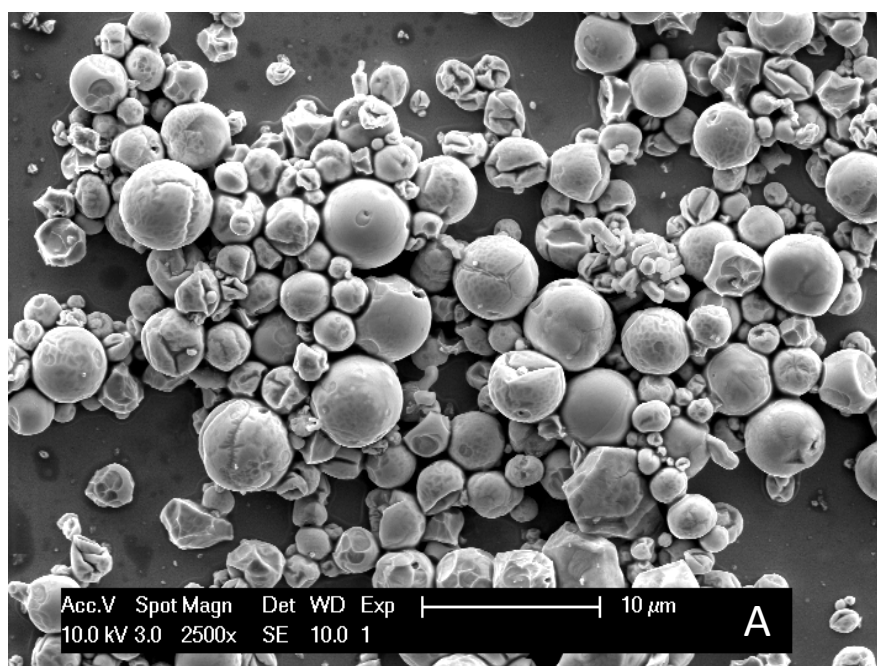


Fig. S21 SEM picture (A) and corresponding EDS spectrum (B) of deposits on a molybdenum working electrode at -2.00 V vs. Fc^+/Fc and at 120 °C for 2 h from purified Cyphos IL 101 loaded with 400 mM of indium(III), 400 mM of zinc(II) and 400 mM of iron(III).

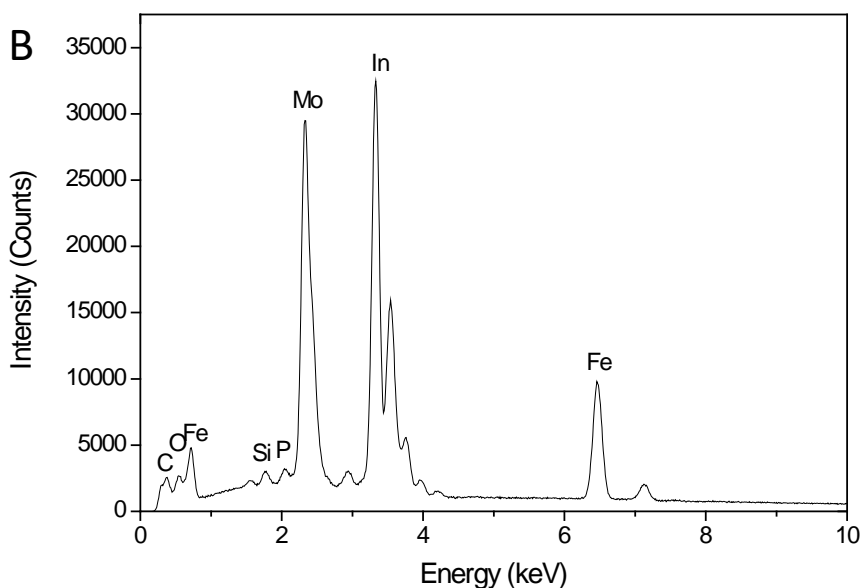
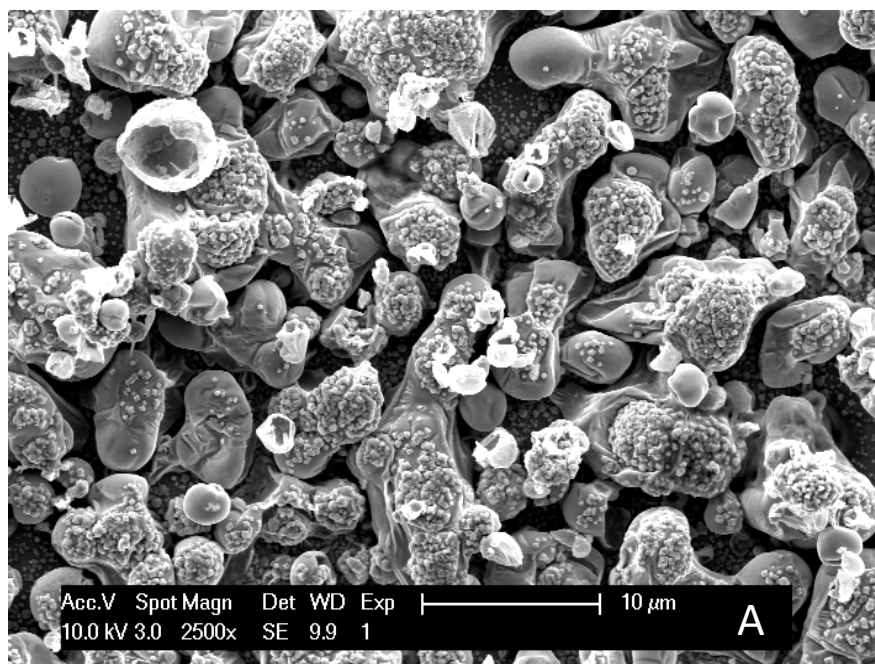


Fig. S22 SEM picture (A) and corresponding EDS spectrum (B) of deposits on a molybdenum working electrode at -2.00 V vs. Fc^+/Fc and at 180 °C for 2h from purified Cyphos IL 101 loaded with 400 mM of indium(III), 400 mM of zinc(II) and 400 mM of iron(III).

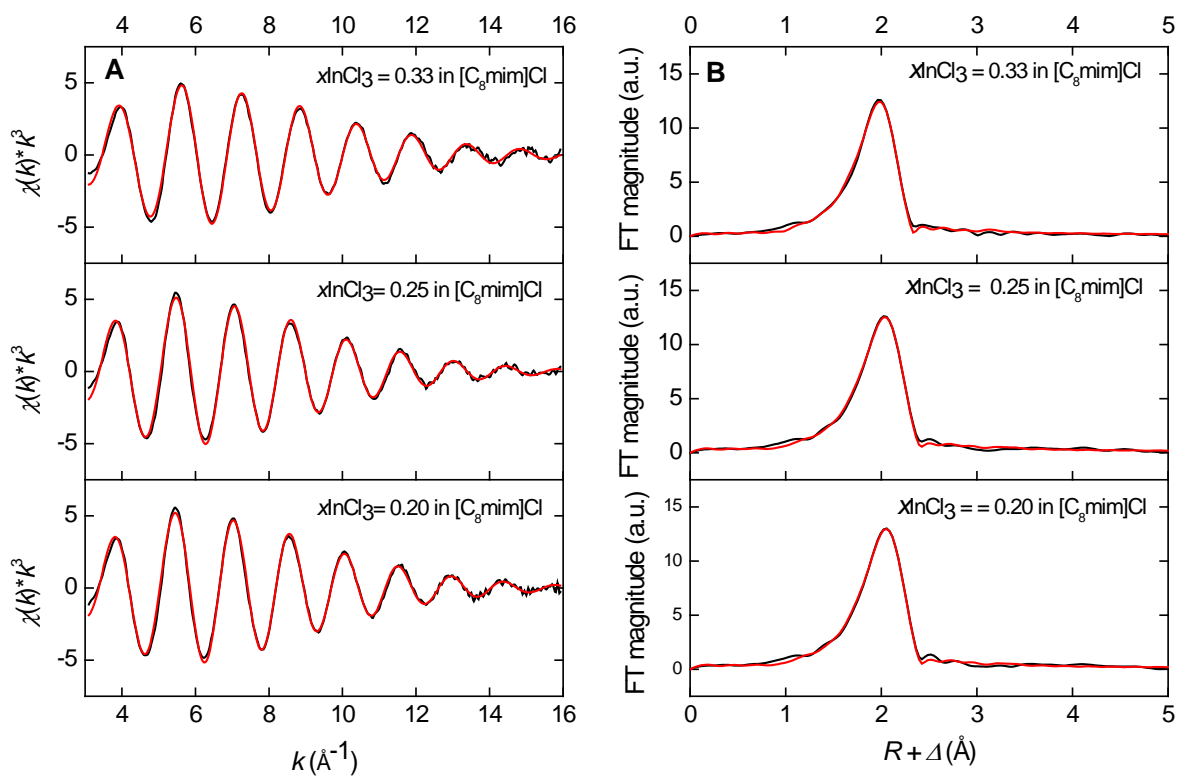


Fig. S23 EXAFS functions (A) and the corresponding FTs (B) indium(III) chloride dissolved in [C₈mim]Cl at three mole fractions $x_{\text{InCl}_3} = 0.33$, 0.25 and 0.20 . Experimental data (black) and theoretical fit (red) are shown.

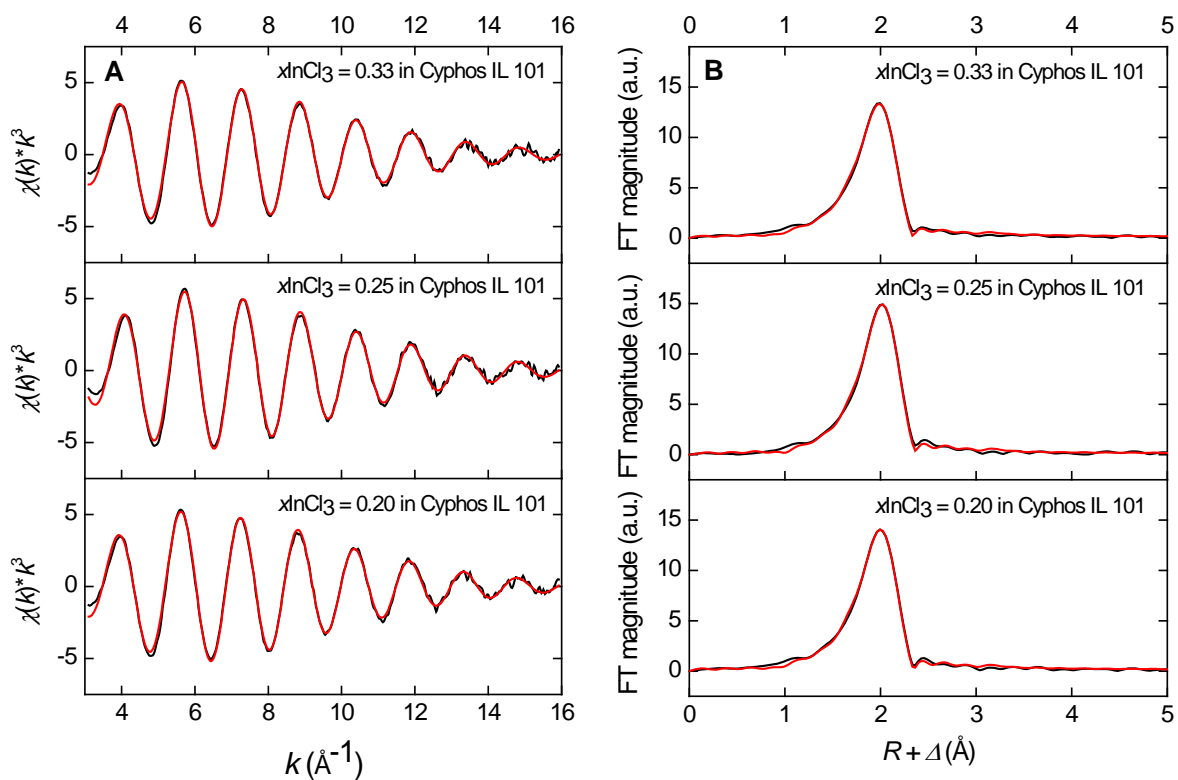


Fig. S24 EXAFS functions (A) and the corresponding FTs (B) indium(III) chloride dissolved in Cyphos IL 101 at three mole fractions $x_{\text{InCl}_3} = 0.33$, 0.25 and 0.20 . Experimental data (black) and theoretical fit (red) are shown.

Diffusion coefficient of indium in purified Cyphos IL 101

The diffusion coefficient of indium (10 mM) in purified Cyphos IL 101 was determined by rotating disk electrode (RDE) voltammetry at 120 °C.[§] The viscosity and density of the electrolyte at 120 °C were extrapolated from experimental values measured between 40 °C and 95 °C.

For the density, a linear fit was applied (Fig. S25†). For the absolute viscosity (η), the Vogel-Fulcher-Tammann model was used (Fig. S26†):

$$\eta = \eta_0 e^{\left(\frac{A}{T-T_F}\right)} \quad (1)$$

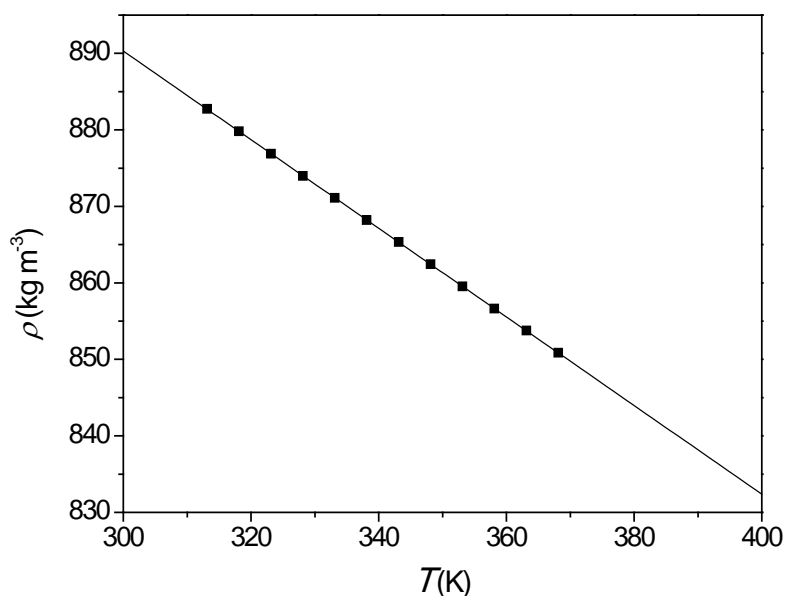


Fig. S25 Density (ρ) of purified Cyphos IL 101 containing 10 mM of indium(III) as a function of the temperature (314–369 K; 40–95 °C). Viscosity values are extrapolated to 300 and 400 K.

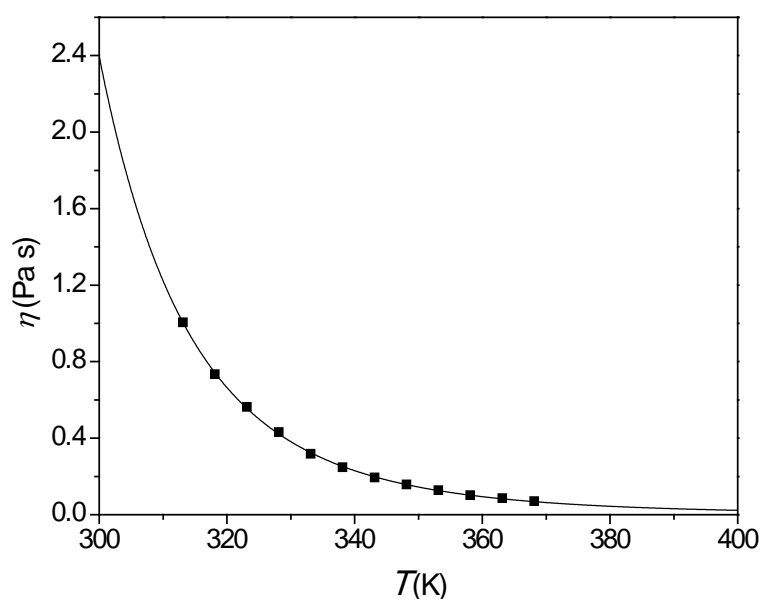


Fig. S26 Viscosity (η) of purified Cyphos IL 101 containing 10 mM of indium(III) as a function of the temperature (314–369 K; 40–95 °C). Viscosity values are extrapolated to 300 K and 400 K.

§ At 180 °C, the deviation in thermal expansion coefficients of the electrode and shroud (PEEK) is too high and the heat distortion temperature of the resin inside the rotating disk electrode is exceeded.^{9–11}

where η_0 is the high temperature viscosity limit (Pa s), A is a material constant (K), T is the temperature (K) and T_F is the Vogel temperature (K). The last parameter is in theory always lower than the glass transition temperature of the liquid ($T_{g,onset} = 203$ K, $T_{g,inflection} = 206$ K (Fig. S27)), which is an indicator of the fit quality. For this fit, the value of the high temperature viscosity limit was fixed and determined using the following equation:¹²

$$\eta_0 = \frac{hN_A\rho}{M} \quad (2)$$

where h is Planck's constant (6.626×10^{-34} J s), N_A is Avogadro's number (6.02×10^{23} mol⁻¹), ρ is the density (kg m⁻³) and M is the molar mass (kg mol⁻¹).

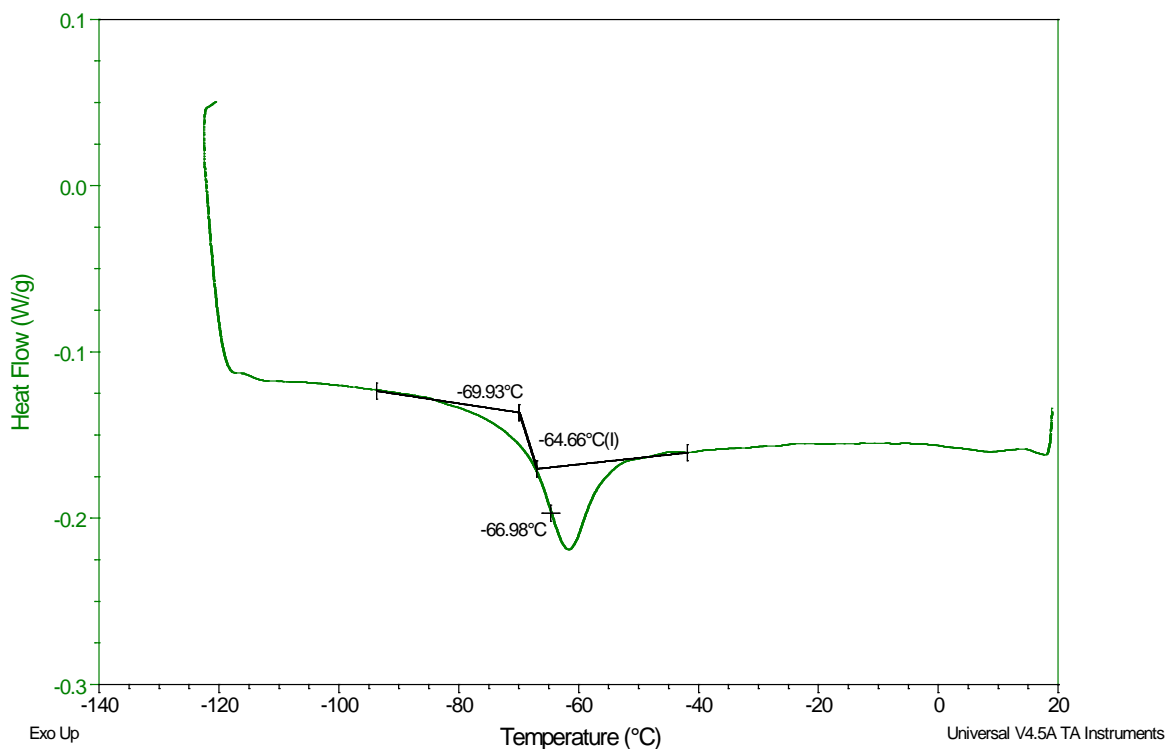


Fig. S27 DSC scan of commercial Cyphos IL 101. Sample mass: 21.40 mg, heating rate: 5 °C min⁻¹, nitrogen gas flow: 60 mL min⁻¹.

Fig. S28 shows the rotating disk electrode linear sweep voltammograms of purified Cyphos IL 101 containing 10 mM of indium(III), recorded at different rotation speeds, at 120 °C and at two different scan rates. In both sets of voltammograms, a reduction wave was observed at around $E = -1.2$ V vs. Fc^+/Fc , which corresponds to the reduction of the remaining impurities present in Cyphos IL 101. This wave is observable because the concentration of indium in solution is of the same order of magnitude as that of the impurity after purification. Interestingly, even when recording at 5 mV s⁻¹, the cathodic current related to the impurity exhibited a peak, indicating that diffusion is hampered. Boxall *et al.* observed similar behavior and attributed it to the viscosity of ionic liquids.¹³ It is possible that a product formed by the reduction of the impurities adsorbs on the electrode, partially blocking it. In the same voltammogram, the reduction of indium (for $E < -1.5$ V vs. Fc^+/Fc) is occurring under time-independent diffusion control, since fairly constant limiting currents are obtained. Since it was not possible to obtain steady state voltammograms, even at lower scan rates, this set of data was used for the determination of the diffusion coefficient. After extracting the limiting currents at -2.12 V vs. Fc^+/Fc from the linear sweep voltammograms

(Fig. S28(B), 120 °C, $v_{\text{scan}} = 20 \text{ mV s}^{-1}$) and plotting them as a function of the square root of the rotation speed, a linear correlation with zero intercept was obtained (Fig. S28). Using the data of Fig. S29, the diffusion coefficient of $[\text{InCl}_6]^{3-}$ was determined using the Levich equation:¹³

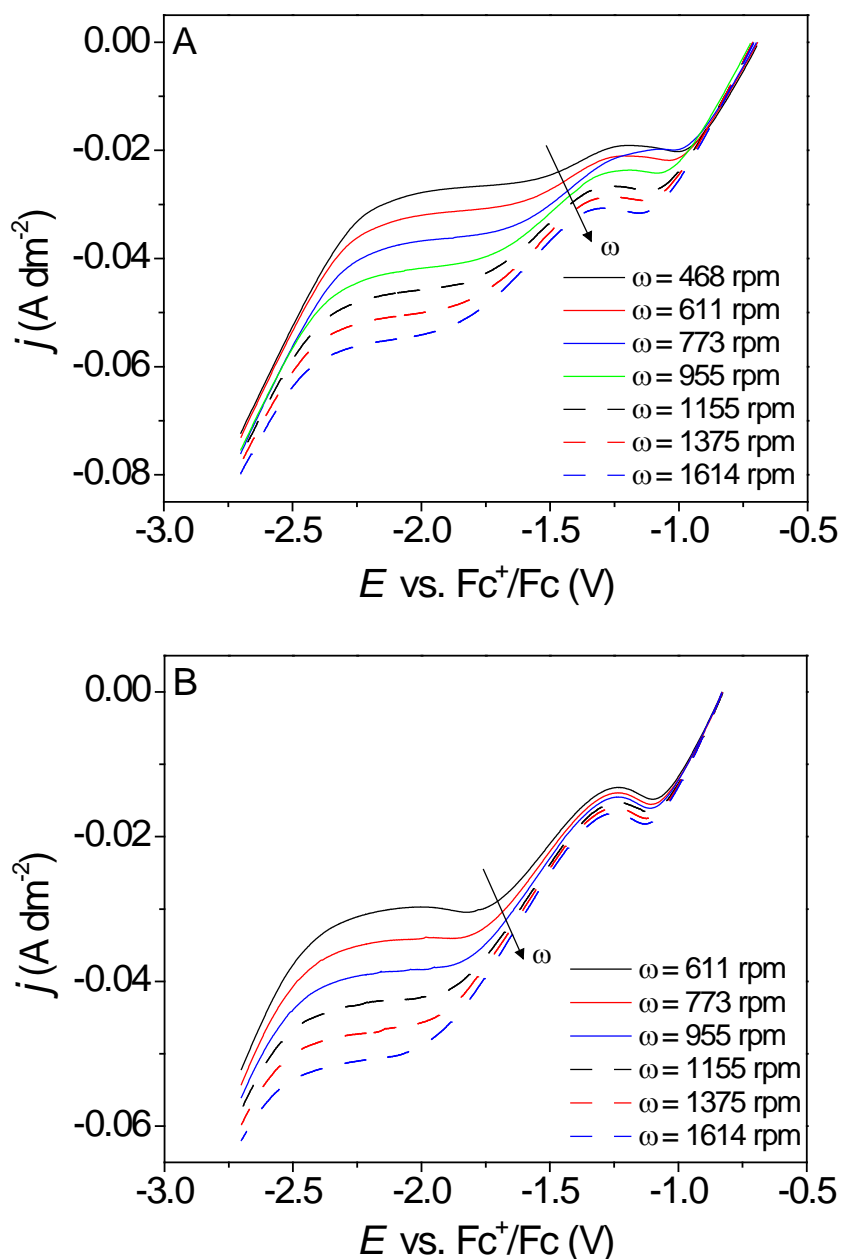


Fig. S28 Rotating disk electrode linear sweep voltammograms of purified Cyphos IL 101 containing 10 mM of indium on a platinum rotating disk electrode (RDE) at 120 °C and recorded with A) $v_{\text{scan}} = 5 \text{ mV s}^{-1}$ and B) $v_{\text{scan}} = 20 \text{ mV s}^{-1}$.

$$i_L = 0.62kFAD_n^{2/3}v^{-1/6}C\omega^{1/2} \quad (3)$$

where, i_L is the limiting current from the linear sweep voltammogram (A), k is the number of electrons transferred (3, dimensionless), F is the Faraday constant ($96485.33 \text{ C mol}^{-1}$), A is the surface area of the electrode ($7.1 \times 10^{-6} \text{ m}^2$), D_n is the diffusion coefficient of the electroactive species ($\text{m}^2 \text{ s}^{-1}$), v is the kinematic viscosity of the electrolyte ($3.3 \times 10^{-5} \text{ m}^2 \text{ s}^{-1}$), C is the

concentration of indium in the electrolyte (10 mol m^{-3}) and ω is the electrode rotation speed (rad s^{-1}). Using the Levich equation a diffusion coefficient of $(7.5 \pm 0.1) \times 10^{-12} \text{ m}^2 \text{ s}^{-1}$ at $120 \text{ }^\circ\text{C}$ was calculated.

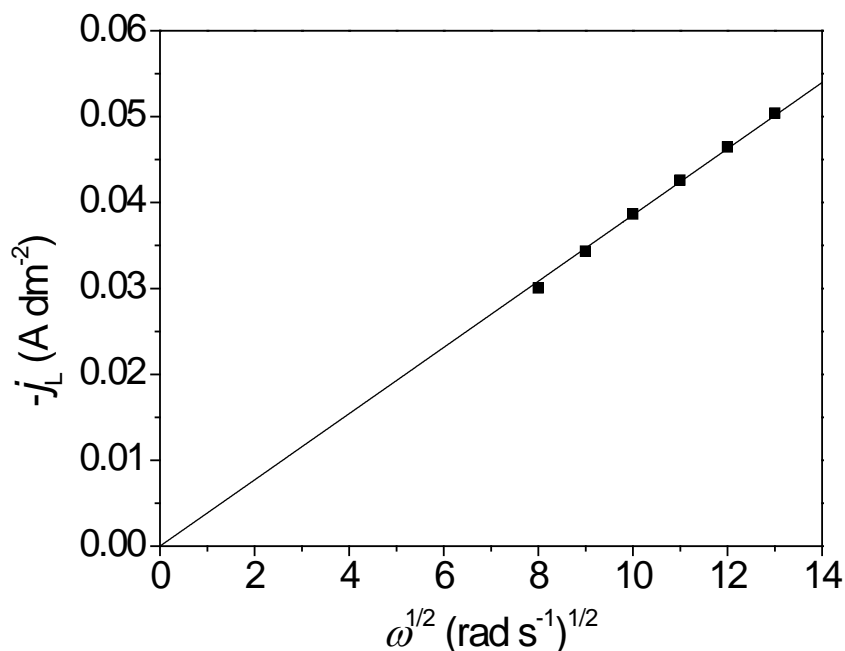


Fig. S29 Levich plot for purified Cyphos IL 101 containing 10 mM of indium. The data were taken from the linear sweep voltammograms recorded at $120 \text{ }^\circ\text{C}$ and $v_{\text{scan}} = 20 \text{ mV s}^{-1}$ at a potential of -2.12 V vs. Fc^+/Fc .

Matsumiya *et al.* determined the diffusion coefficient for several trivalent and divalent complexes in the ionic liquid triethyl-*n*-pentylphosphonium bis(trifluoromethylsulfonyl)-imide, $[\text{P}_{2225}][\text{Tf}_2\text{N}]$, at $25 \text{ }^\circ\text{C}$ (Table S1).^{14,15} These diffusion coefficients are of the same order as for indium(III) complexes in purified Cyphos IL 101 at $120 \text{ }^\circ\text{C}$. The low diffusion coefficient of indium(III) in purified Cyphos IL 101, in comparison with several trivalent and divalent metal complexes in $[\text{P}_{2225}][\text{Tf}_2\text{N}]$, can be explained by their difference in viscosity. The viscosity of Cyphos IL 101 is almost 34 times higher than that of $[\text{P}_{2225}][\text{Tf}_2\text{N}]$ at $25 \text{ }^\circ\text{C}$ (Table S2). At $120 \text{ }^\circ\text{C}$, the viscosity of Cyphos IL 101 is equal to 28.3 mPa s^{-1} , which is in the same order of magnitude as the viscosity of $[\text{P}_{2225}][\text{Tf}_2\text{N}]$ at $25 \text{ }^\circ\text{C}$. Besides the viscosity, the ionic conductivity of Cyphos IL 101 is also very different compared to $[\text{P}_{2225}][\text{Tf}_2\text{N}]$. It is estimated that at $25 \text{ }^\circ\text{C}$, the ionic conductivities of purified Cyphos IL 101 and $[\text{P}_{2225}][\text{Tf}_2\text{N}]$ will differ by almost three orders of magnitude.

Table S1 The diffusion coefficient D of some trivalent and divalent complexes in triethyl-*n*-pentylphosphonium bis(trifluoromethylsulfonyl)imide, [P₂₂₂₅][Tf₂N], at 25 °C.^{14,15}

Ionic Liquid	Species	Method	$D/10^{-12}$ (m ² s ⁻¹)
[P ₂₂₂₅][Tf ₂ N]	Eu(III)	CA	2.6
		CP	2.4
	Sm(III)	CA	2.8
		CP	2.4
	Dy(III)	SI	2.0
	[PdCl ₄] ²⁻	CV	12 ± 3
		CP	10 ± 3
	[PdBr ₄] ²⁻	CV	6 ± 2
		CP	5 ± 2

Table S2 Viscosity (η) and ionic conductivity (σ) of [P₆₆₆₁₄]Cl and triethyl-*n*-pentylphosphonium bis(trifluoromethylsulfonyl)imide, [P₂₂₂₅][Tf₂N].^{16,17}

Ionic Liquid	η (mPa s)	σ (mS cm ⁻¹)
[P ₆₆₆₁₄]Cl	4277 ± 50 (20 °C) ^a , 2887 ± 48 (25 °C) ^a	2.5 × 10 ⁻³ (20 °C)
[P ₂₂₂₅][Tf ₂ N]	85.30 (25 °C)	2.10 (25 °C)

^a This work

Notes and references

- 1 G. Vanhoutte, M. Wu, S. Schaltin, F. Mattelaer, C. Detavernier, P. M. Vereecken, K. Binnemans and J. Fransaer, *J. Mater. Chem. A*, 2016, **4**, 13555–13562.
- 2 A. Lewandowski, L. Waligora and M. Galinski, *Electroanalysis*, 2009, **21**, 2221–2227.
- 3 P. De Vreese, K. Haerens, E. Matthijs and K. Binnemans, *Electrochim. Acta*, 2012, **76**, 242–248.
- 4 P. Lobaccaro, A. Raygani, A. Oriani, N. Miani, A. Piotto, R. Kapadia, M. Zheng, Z. Yu, L. Magagnin D. C. Chrzan, R. Maboudian and A. Javey, *J. Electrochem. Soc.*, 2014, **161**, D794–D800.
- 5 S. Nikitenko, A.M. Beale, A.M. van der Eerden, S.D. Jacques, O. Leynaud, M.G. O'Brien, D. Detollenaere, R. Kaptein, B.M. Weckhuysen and W. Bras, *J Synchrotron Radiat.*, 2008, **15**, 632–640.
- 6 K. V. Klementev, *Nucl. Instrum. Methods Phys. Res., Sect. A*, 2000, **448**, 299–301.
- 7 M. Newville, *J. Synchrotron Radiat.*, 2001, **8**, 96–100.
- 8 C. Deferm, A. Van den Bossche, J. Luyten, H. Oosterhof, J. Fransaer and K. Binnemans, *Phys. Chem. Chem. Phys.*, 2018, **20**, 2444–2456.
- 9 M. J. Fleige, G. K. H. Wiberg and M. Arenz, *Rev. Sci. Instrum.*, 2015, **86**, (064101-1)–(064101-6).
- 10 S. X. Lu, P. Cebet and M. Capel, *Polymer*, 1996, **37**, 2999–3009.
- 11 R. K. Kirby, *Int. J. Thermophys.*, 1991, **12**, 679–685.
- 12 S. C. Glade and W. L. Johnson, *J. Appl. Phys.*, 2000, **87**, 7249–7251.
- 13 D. L. Boxall, J. J. O'Dea and R. A. Osteryoung, *J. Electrochem. Soc.*, 2002, **149**, E468–E471.
- 14 M. Matsumiya, S. Suda, K. Tsunashima, M. Sugiya, S. Kishioka and H. Matsuura, *J. Electroanal. Chem.*, 2008, **622**, 129–135.
- 15 A. Kurachi, M. Matsumiya, K. Tsunashima and S. Kodama, *J. Appl. Electrochem.*, 2012, **42**, 961–968.
- 16 C. Pozo-Gonzalo, P. C. Howlett, J. L. Hodgson, L. A. Madsen, D. R. MacFarlane and M. Forsyth, *Phys. Chem. Chem. Phys.*, 2014, **16**, 25062–25070.
- 17 V. L. Martins, N. Sanchez-Ramirez, M. C. C. Ribeiro, R. M. Torresi, *Phys. Chem. Chem. Phys.*, 2015, **17**, 23041–23051.